Journal of Cancer Therapy and Research

Genesis-JCTR-1(1)-08
Volume 1 | Issue 1
Open Access
ISSN: 2583-6552

Evaluating the Impact of CT Scanning Parameters on Dose Calculations by the Treatment Planning System in External Beam Radiation Therapy

Barrington A Brevitt[1*], Edwin Ges Suarez[2], Rafael A Miller Clemente[3] and Mitko Voutchkov[1]

[1]Department of Physics, The University of the West Indies, Mona, Kingston 7, Jamaica
[2]National Cancer Treatment Centre, Kingston 3, Jamaica
[3]Center of Medical Biophysics, Western University, 90400, Santiago de Cuba, Cuba

[*]**Corresponding author:** Barrington A Brevitt, Department of Physics, The University of the West Indies, Mona, Kingston 7, Jamaica.

Citation: Brevitt BA, Suarez EG, Clemente RAM, Voutchkov M. (2021) Avoiding Defensive Medicine among Pandemic. J Can Ther Res. 1(1):1-16.

Received: November 03, 2021 | **Published**: November 28, 2021

Abstract

This study sought to evaluate scanning parameters for Computed Tomography (CT) simulations and its impact on dose calculation by a treatment planning systems. A Computerized Imaging Reference System (CIRS) electron density phantom was scanned with a GE multi-detector scanner to acquire 1.25 mm slices in helical mode. Evaluations were done with the standard image reconstruction using a circular region of interest (ROI) from the measuring tool of the workstation software. Radiation therapy plans were prepared using the Eclipse Treatment Planning System (TPS) and an analysis of the influence of the scanning parameters over dose calculation was done. Scanning parameters can affect the dose calculation resulting in deviations between the TPS and Hounsfield Unit- relative electron density (HU-ED_r) calibration curve. Such deviations may lead to uncertainties in the calculation of output dose in the radiotherapy plan. Changes in kilo-voltage peak (kVp) had a direct impact on the HU measured for each tissue-equivalent insert. The effects of different tube voltages on the HU for various tissue substitutes in the phantom, and their dosimetric impact on dose calculation in TPS is due to variations in the HU-EDr calibration curve.

DOI: *https://doi.org/10.52793/JCTR.2021.1(1)-08*

The technical factors selected for scanning has a direct impact on the HU value obtained from the scan data. This in turn affects HU-EDr calibration and radiation therapy dose calculations.

Keywords
Hounsfield units; Relative electron density; Monte carlo; Linear attenuation; Tissue maximum ratio (TMR).

Introduction

The quality of Computed Tomography (CT) images influence the recognition and delineation of target volumes and the surrounding organs at risk (OARs). Substandard image quality may result in improper delineation of the target volume and OARs by omission of the target or over-inclusion of a portion of normal organ volumes. Thus, it is essential to evaluate the image quality of CT scanners used for simulation of radiotherapy patients. The accuracy of dose calculation by the radiotherapy Treatment Planning System (TPS), takes into account the effect of tissue inhomogeneities based on CT data and the calibration of CT Hounsfield Unit (HU) and Relative Electron Density (ED_r) curves. CT number or HU provides information on the attenuation characteristics of X-ray beam in a particular volume element in the patients' body with respect to that of water at a specific kilo-voltage peak (kVp).

The images obtained from CT can be used in radiation oncology as a basis for dose distribution when treatment plans are being prepared for internal or external radiation therapy. As x-rays traverse the patients' body, they interact with tissue of varying densities giving rise to Compton and Photoelectric scattering. These interactions are dependent on the photon energy; the effective atomic number and the electron density of the medium. Photons ranging in energies of 0.3-2 MeV undergo the Compton Effect and those that are less or in excess of this energy range are involved in the Photoelectric Effect or other photon-matter interactions respectively. These scattered photon energies give rise to photon fluence which can be used to estimate the electron densities (ED) of tissue along the path traversed by the beam. Table 1 highlights the various inhomogeneities encountered by the treatment beam as it traverses the patient's body to the target volume. These differences create a heterogeneous environment requiring precise and accurate treatment planning and dose delivery.

Tissue	Typical HU	Typical Thickness (cm)	ED_r	Product of t and (ED_r^{-1})
Lung	-740	8	0.26	-5.92
Fat	-50	4	0.95	0.20
Liver	50	8	1.05	0.40
Rib	600	1	1.34	0.34
Humerus	700	2.5	1.39	0.98
Cranium	900	1.5	1.51	0.77

Table 1: Typical inhomogeneities encountered in treatment planning and changes in water equivalent thickness

DOI: *https://doi.org/10.52793/JCTR.2021.1(1)-08*

caused by inhomogeneity.

Electron Density (ED) is defined as the number of electrons contained by tissue of specific density expressed in electrons/cm^3. When the electron density of tissue (ED_t) is compared to the electron density of water (ED_w) it results in a ratio referred to as the relative electron density (ED_r). It is known that a relationship exists between ED_r and the HU generated for each pixel of a CT scan [1]. The HU is generated for each pixel of the CT cross-sectional image resulting from the linear attenuation of x-rays as they interact with different tissue densities within the body. HU is the difference of the linear attenuation of tissue within a pixel and the linear attenuation of water within a similar pixel, and is calculated from:

$$\mathrm{HU} = 1000 \times \left(\frac{\mu_t - \mu_w}{\mu_w}\right) \qquad (1)$$

Where: (μ_t) is the linear attenuation of tissue and (μ_w) is the linear attenuation of water. Attenuation coefficients depend on electron density, atomic number (Z) and the quality of the beam used for the scan [2]. Computed tomography in radiation therapy has three applications; it is used for the acquisition of patient images and tumors contours; it is employed to evaluate the results of treatment and for obtaining density information concerning the patient to improve the accuracy of dose calculations. The construction of a CT scanner generates systematic errors due to beam hardening and the detection of scattered radiation. In early generation scanners, these errors usually manifest as an increasing density towards the centre of the image known as the cupping effect [3]. In later generation scanners corrections are done by a process of linearizing the x-ray transmission data.

Scanners generate HU which are physical quantities allowing universal characterization of human tissue for diagnostic purposes and heterogeneity corrections in radiation therapy planning. The polychromatic x-ray source used in CT coupled with a broad energy response detector prevents the separate detection of primary and scattered radiation. Scanners are constructed to reduce the degree of scattering reaching the detector; however, for scattered rays detected they create errors in the determination of the linear attenuation coefficient. In radiation therapy planning, a patient's body is compared to water of variable effective densities, corresponding to electron density for high energy photons or stopping power ratio for charged particles. As cancer treatment and technology evolves, the use of simulation CTs is becoming more prevalent, where radiation is utilized as an assortment of particles interacting with tissue of known composition and used for Monte Carlo (MC) calculations. For patient dose calculations the TPS uses MC functions to convert HU to effective densities of interest. For other analytical dose calculation algorithms e.g. AAA, the TPS uses HU-electron density calibration curves for this conversion. In algorithms such as Acuros XB, the TPS uses the HU value-density calibration curves to convert HU to the material composition. The HUs are converted to ED that is automatically converted to interaction-specific effective densities using invariant associations [4]. This proves the importance of accurate representation of ED within the TPS and the scanning system, as inaccuracies can result in calculation errors.

Methodology

Scans of a Computerized Imaging Reference System (CIRS) electron density phantom (model 062M) were acquired with a GE Optima 16 slice multi-detector (MD) scanner with the scanning parameters outlined

DOI: *https://doi.org/10.52793/JCTR.2021.1(1)-08*

in Table 2. The distribution of the tissue-equivalent inserts within the phantom is shown in Figure 1, while Table 3 outlines the different densities of the inserts used to acquire HU and standard deviation (SD) measurements.

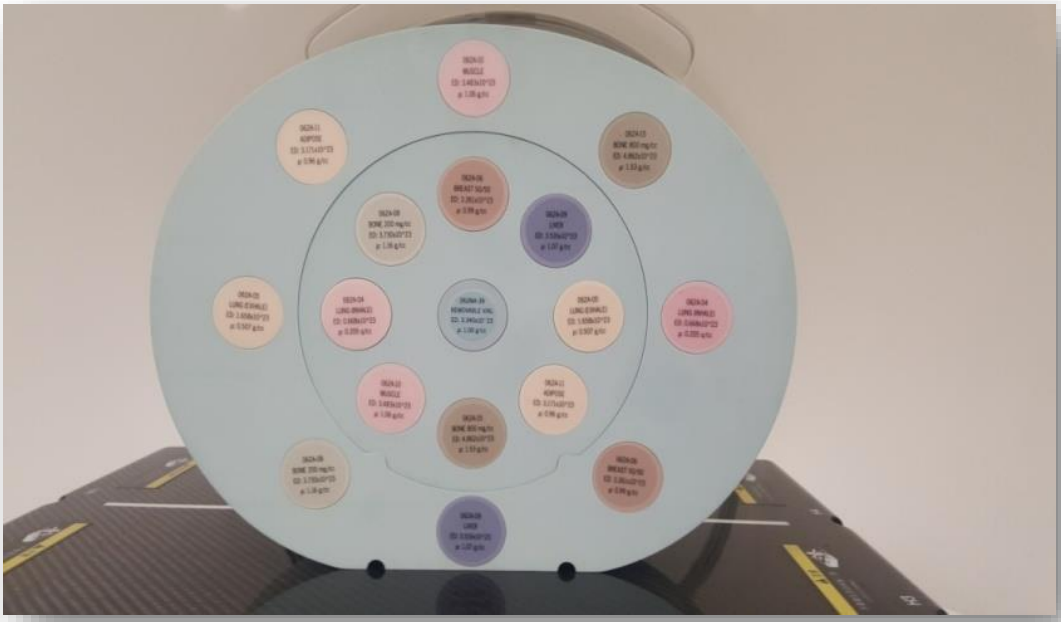

Figure 1: Distribution of tissue-equivalent inserts in CIRS phantom.

The phantom was aligned using external wall and ceiling lasers as seen in Figure 2 and the first set of scans were acquired at tube voltages of 80, 100, 120 and 140 kVp respectively, with the tube current set at 400 mA. The second set of scans was acquired with the tube voltage set at 120 kVp while varying the tube current. The values used were 100, 200, 300, 400 and 440 mA respectively.

Slice thickness	1.25 mm
Window Width / Window Level	350/40
Pitch	0.938:1
Tilt	0^0
Recon Type	Standard
DFOV	41.8 cm
Matrix size	512
SFOV	Large Head
Scan Type	Helical

Table 2: Scan acquisition parameters.

DOI: *https://doi.org/10.52793/JCTR.2021.1(1)-08*

Figure 2: Set-up of the phantom using external lasers.

Three scans were done at each kVp and mA setting to account for uncertainties in measurements. The measuring tool on the view station was used to select a circular ROI (444.47 mm^2) with a diameter of 24 mm to evaluate the mean Hounsfield Unit and standard deviation of each tissue-equivalent insert for each tube voltage and current setting. Calibration curves were compared to theoretical curves calculated by Varian, which was pre-set in the Eclipse TPS and were considered as a reference 5 [5].

$$HU < 100: ED_r = 1 + (1.001 \times HU) \quad (2)$$

$$HU > 100: ED_r = 1.052 + (0.00048 \times HU) \quad (3)$$

The scan images were transferred to the Eclipse TPS version 15.0 and processed using the contouring tool. Subsequent to image transfer a fusion was done and the recommended quality assurance tests were performed as seen in Figure 3. The fused images were then employed to conduct typical radiotherapy planning techniques such as 3-Dimensional Radiation Therapy (3DRT) and Volumetric Modulated Arc Therapy (VMAT) which is an inverse planning technique as shown in Figure 7 and Figure 8. This was done to evaluate the influence of the ED_r assumed by the TPS in the dose calculation process.

Tissue Equivalent Material (density plugs)	Physical Density (g/cc)	Electron Density (x 10^{23} electrons/cc)	ED_r (relative to water)
Lung Inhale	0.205	0.668	0.200
Lung Exhale	0.507	1.658	0.496
Adipose	0.96	3.171	0.949
Breast (50% gland/ 50% Adipose)	0.99	3.261	0.976
Muscle	1.06	3.483	1.043
Liver	1.07	3.516	1.052
Solid Trabecular Bone (200 mg/cc HA)	1.16	3.730	1.117

DOI: *https://doi.org/10.52793/JCTR.2021.1(1)-08*

Solid Dense Bone (800 mg/cc HA)	1.53	4.862	1.456

Table 3: Phantom Specifications.

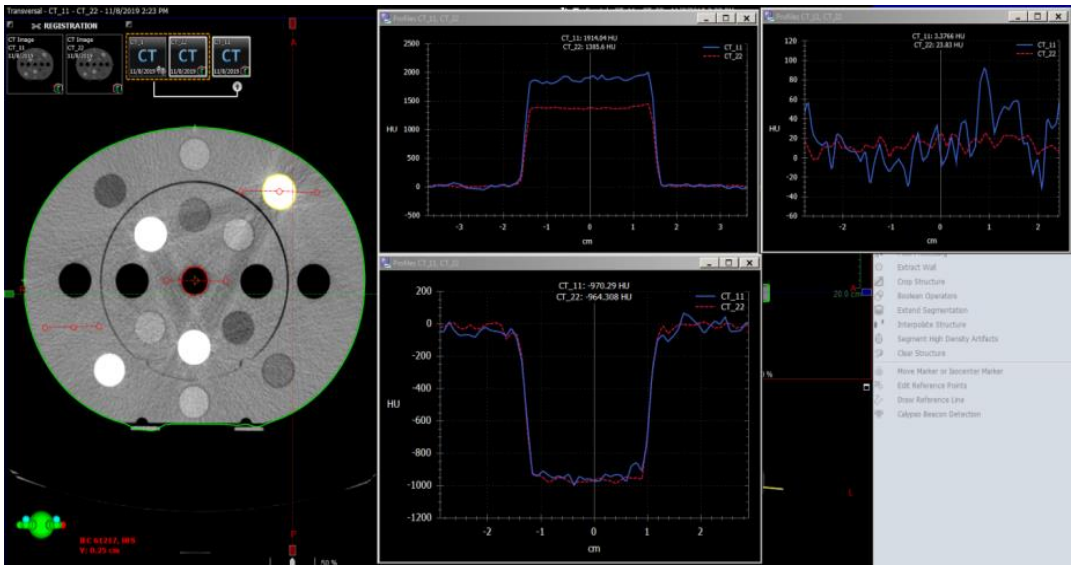

Figure 3: Profile of Fused Images at 80 and 140 kVp.

Results

It was found as illustrated in Table 4 that changes in kVp had a direct impact on the HU measured for each tissue-equivalent insert. Changes in kVp and mA also had effects on the ED_r of the tissue inserts. HU analysis by the TPS of imported images, yielded results consistent with those obtained from the scanner software before images were imported. Figure 3 shows profiles generated when image fusion was done with phantom images obtained at 80 kVp and 140 kVp. This analysis highlighted a disparity with the HU measured for high density material. A direct relationship between kVp and ED_r was observed, as increases in the tube voltage resulted in a corresponding rise in ED_r. This relationship was not apparent with tube current. As the mA increased there were negligible changes in ED_r producing a uniform curve as shown in Figure 4 and Figure 5 respectively.

DOI: *https://doi.org/10.52793/JCTR.2021.1(1)-08*

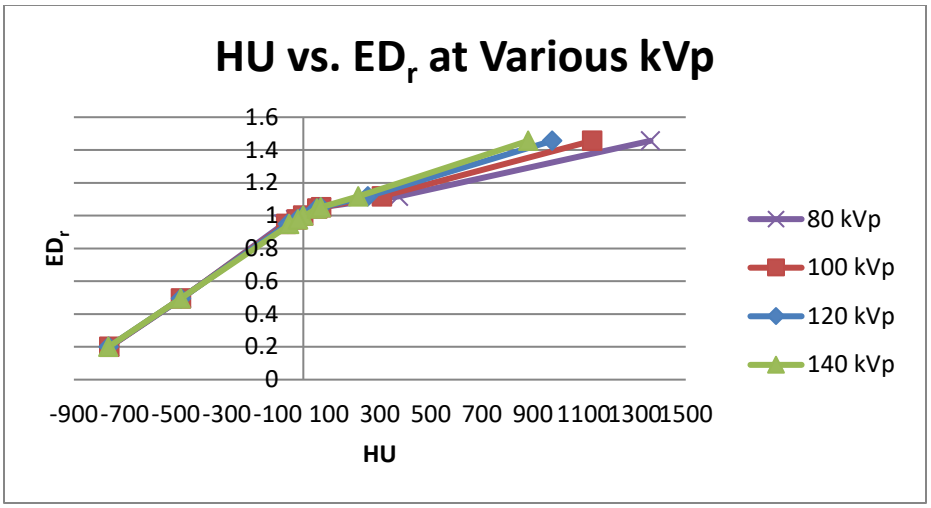

Figure 4: HU vs. ED_r at various kVp.

Tissue Equivalent Material	HU Recorded (80 kVp)	HU Recorded (100 kVp)	HU Recorded (120 kVp)	HU Recorded (140 kVp)
Lung Inhale	-759.45	-760.92	-763.09	-763.71
Lung Exhale	-476.97	-478.89	-479.51	-480.07
Adipose	-76.86	-66.46	-60.65	-55.65
Breast (50% gland/ 50% Adipose)	-30.40	-24.67	-22.33	-19.57
Muscle	55.6	55.19	53.14	53.82
Liver	71.51	69.86	68.65	68.53
Solid Trabecular Bone (200 mg/cc HA)	374.15	309.05	253.8	216.07
Solid Dense Bone (800 mg/cc HA)	1361.94	1133.37	976.15	882.24

Table 4: Changes in kVp and corresponding HU.

Figure 6 illustrates that for tissues with an electron density less than that of water, namely; lung, adipose and breast there was a corresponding rise in HU value with increases in kVp. The largest change in HU occurred in breast tissue when HU values obtained at 80 kVp and 140 kVp were compared, where a 35.6% difference was observed. The smallest change was obtained in the simulated lung tissue. For tissues with densities greater than water, namely; muscle, liver and bone there was an inverse relationship. As the kVp value increased the HU decreased. The largest decline in mean HU was observed in solid bone material and the smallest change was observed in the muscle simulating material.

Doses calculated with the images of the phantom acquired using kVp values of; 80, 100, 120, and 140, and applying the HU-ED_r curve generated from a tube voltage of 120 kVp were within 1% of the expected dose. Figure 7 and Figure 8 show dose evaluation on the Eclipse TPS for different interest points for plans

DOI: *https://doi.org/10.52793/JCTR.2021.1(1)-08*

created with a prescription dose of 200 cGy at the isocenter. A 6 MV photon beam was employed to create 3D and VMAT plans respectively for different HU-ED_r curves for various tube voltages. The maximum percentage difference in the dose evaluated at five interest points were 0.82%, 0.64%, for the TPS calculations performed with, AAA and pencil beam algorithms respectively. These interest points were all within the acceptable range; however, differences were greater for the higher density inserts. Differences in the ED_r of high density structures influence the dose calculated by the TPS. Figure 7 and Figure 8 further demonstrates how high density structures can result in an increase in the estimated dose when they are located within the beam path.

Overall it was discovered that the HU value of all tissue rose with increases in tissue density regardless of the tube voltage used to acquire scans. Changes in kVp also caused changes in the SD measured as seen in Table 5. It was also revealed that, as the density of the tissue increased the SD also rose as seen in Figure 9; however, raises in kVp resulted in a fall off of the measured SD. It was noted that at the lower kVp values the SDs were relatively close, but subsequent to kVp exceeding 100 the deviation was more perceptible.

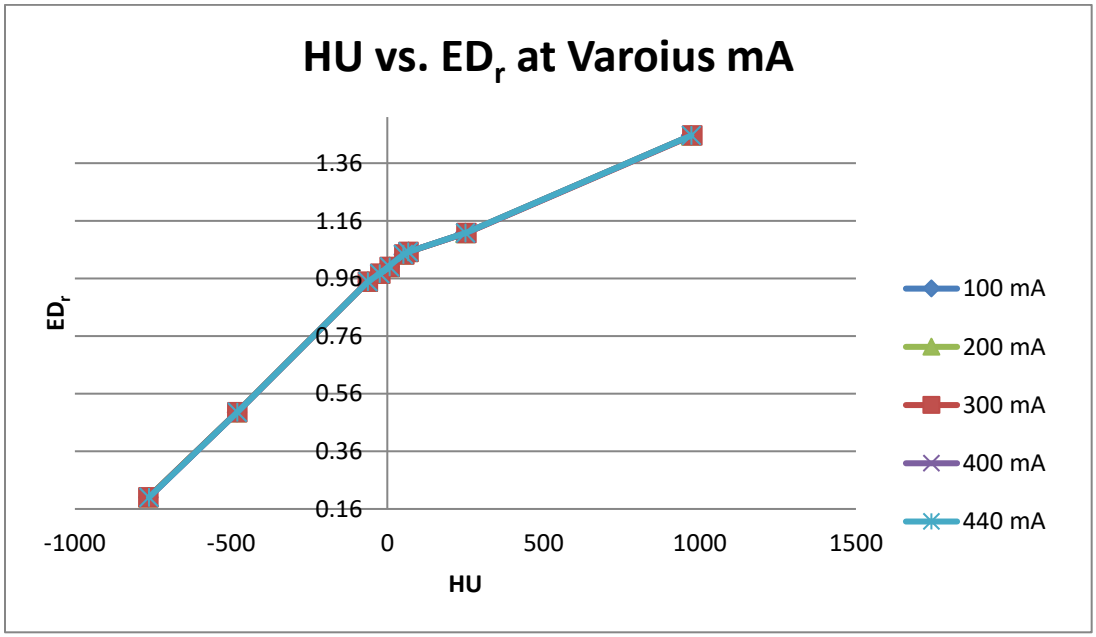

Figure 5: HU vs. relative electron density at different mA.

Tissue Equivalent Material	SD Recorded (80 kVp)	SD Recorded (100 kVp)	SD Recorded (120 kVp)	SD Recorded (140 kVp)
Lung Inhale	36.25	24.29	17.81	15.17
Lung Exhale	39.50	25.71	17.74	16.04
Adipose	46.23	25.99	19.15	15.34

DOI: *https://doi.org/10.52793/JCTR.2021.1(1)-08*

Breast (50% gland/ 50% Adipose)	45.25	26.14	20.02	16.03
Muscle	42.79	26.10	18.57	15.66
Liver	43.72	27.59	18.81	17.48
Solid Trabecular Bone (200 mg/cc HA)	49.45	30.54	22.80	18.53
Solid Dense Bone (800 mg/cc HA)	62.71	35.45	26.20	21.74

Table 5: Changes in kVp and corresponding standard deviation.

Variations in mA had a smaller effect on HU measured, there was an overall decline in HU has mA increased. However, changes ranged from 0.1 to 2 HUs with variations in mA between 100 and 440. At 300 mA tissues with densities greater than the density of water had an increase of HU from that measured at 200 mA.

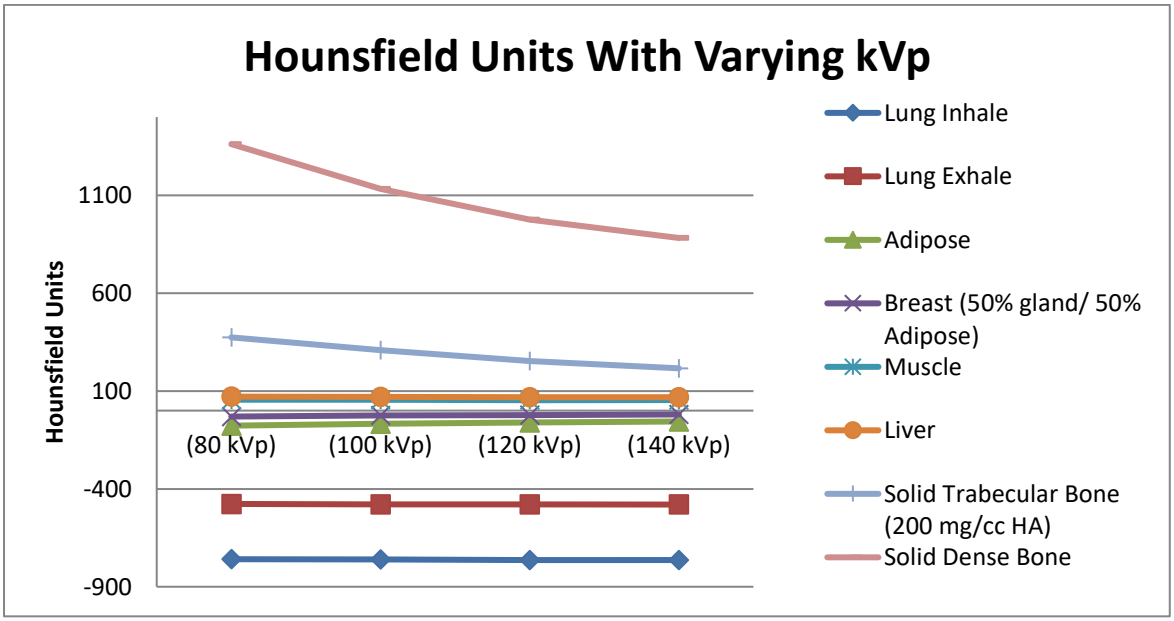

Figure 6: Changes in kVp and the corresponding change in Hounsfield Units.

Tissue Equivalent Material	HU Recorded (100mA)	HU Recorded (200mA)	HU Recorded (300mA)	HU Recorded (400mA)	HU Recorded (440mA)
Lung Inhale	-765.07	-765.05	-764.4	-762.61	-763.08
Lung Exhale	-481.17	-481.04	-480.21	-480.05	-479.67
Adipose	-61.98	-61.78	-61.97	-62.69	-62.32

DOI: *https://doi.org/10.52793/JCTR.2021.1(1)-08*

Breast (50% gland/ 50% Adipose)	-23.49	-23.10	-22.13	-24.18	-24.12
Muscle	52.43	52.36	54.12	51.9	51.73
Liver	67.44	67.47	68.04	66.86	66.51
Solid Trabecular Bone (200 mg/cc HA)	249.35	250.12	253.63	250.95	250.35
1 Solid Dense Bone (800 mg/cc HA)	972.73	972.67	976.66	973.06	973.37

Table 6: Changes in mA and corresponding HU.

The largest rise was seen in bone and it was also identified that above 300 mA changes in HU, as mA increased were negligible; this is represented in Table 6 and Figure 10. At low tube current (100 mA-200 mA) there was a minute increase in SD for all tissue except air-filled lung. The SD, however, decreased between 300 mA and 440 mA. The largest change in SD for most tissue was obtained between 200 mA through 400 mA. This behavior was not seen in air-filled lung as there was a corresponding decrease in SD as mA increased as seen in Table 7 and Figure 11.

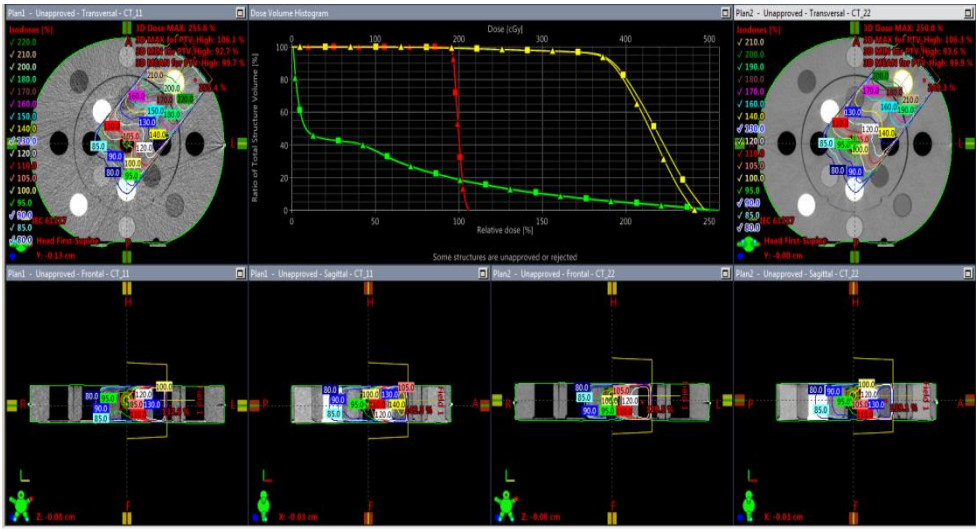

Figure 7: Doses evaluated for 3D on Eclipse TPS.

Tissue Equivalent Material	SD Recorded (100mA)	SD Recorded (200mA)	SD Recorded (300mA)	SD Recorded (400mA)	SD Recorded (440mA)
Lung Inhale	27.86	22.78	19.23	16.75	16.02
Lung Exhale	23.96	24.11	20.47	17.43	16.21

DOI: *https://doi.org/10.52793/JCTR.2021.1(1)-08*

Adipose	26.22	26.32	21.40	17.68	16.9
Breast (50% gland/ 50% Adipose)	26.27	26.34	22.46	18.88	17.17
Muscle	25.36	25.35	21.33	17.86	17.36
Liver	26.16	26.21	21.56	18.66	18.05
Solid Trabecular Bone (200 mg/cc HA)	30.92	30.86	27.32	22.68	21.68
Solid Dense Bone (800 mg/cc HA)	33.53	33.84	29.78	24.19	23.59

Table 7: Changes in mA and corresponding standard deviations.

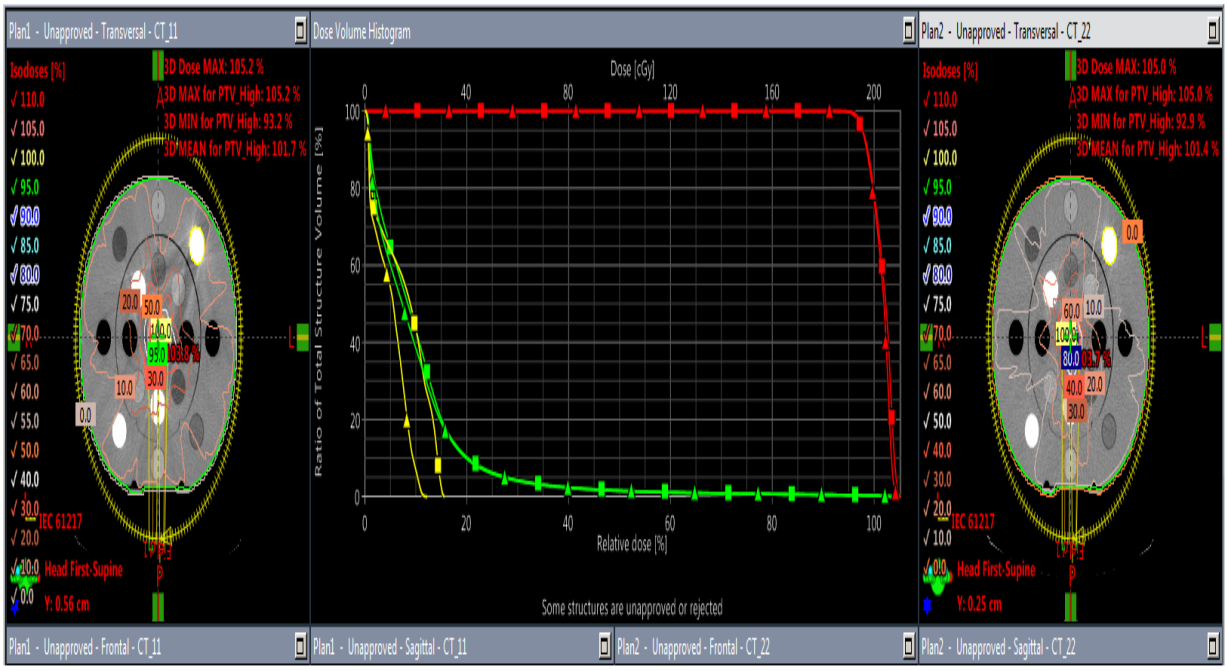

Figure 8: Doses evaluated for VMAT on Eclipse TPS.

DOI: *https://doi.org/10.52793/JCTR.2021.1(1)-08*

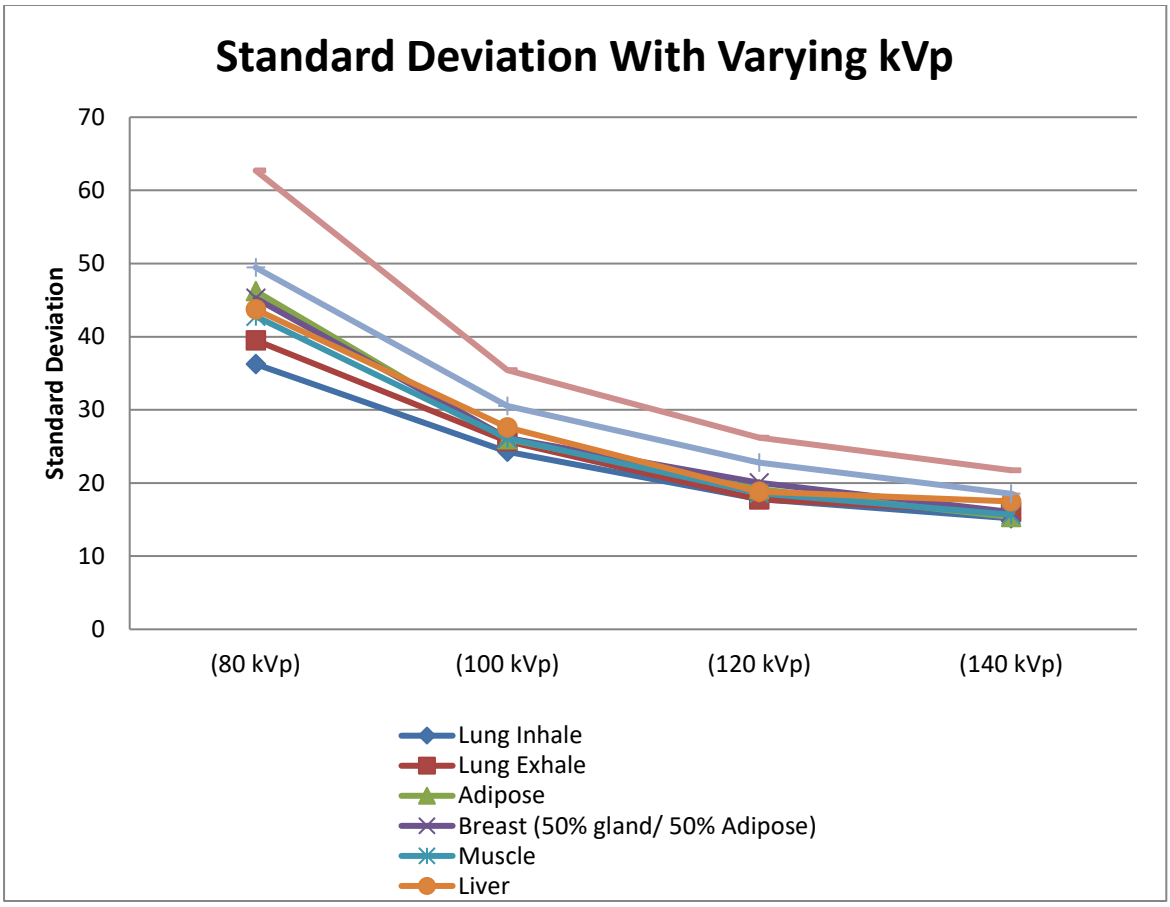

Figure 9: Changes in kVp and the corresponding change in Standard Deviation.

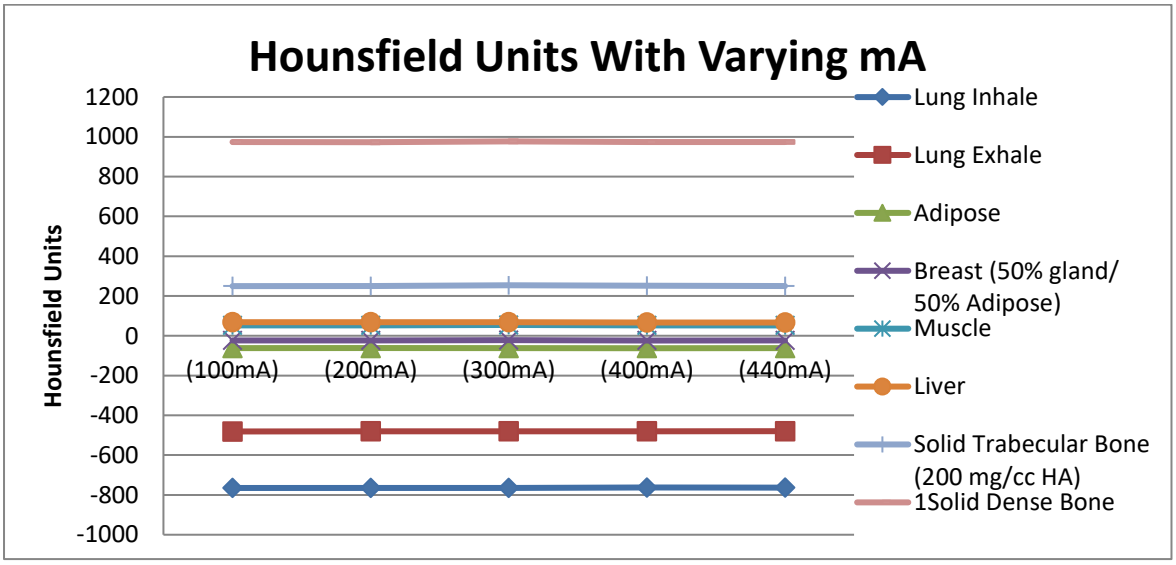

Figure 10: Changes in mA and the corresponding change in Hounsfield Units.

DOI: *https://doi.org/10.52793/JCTR.2021.1(1)-08*

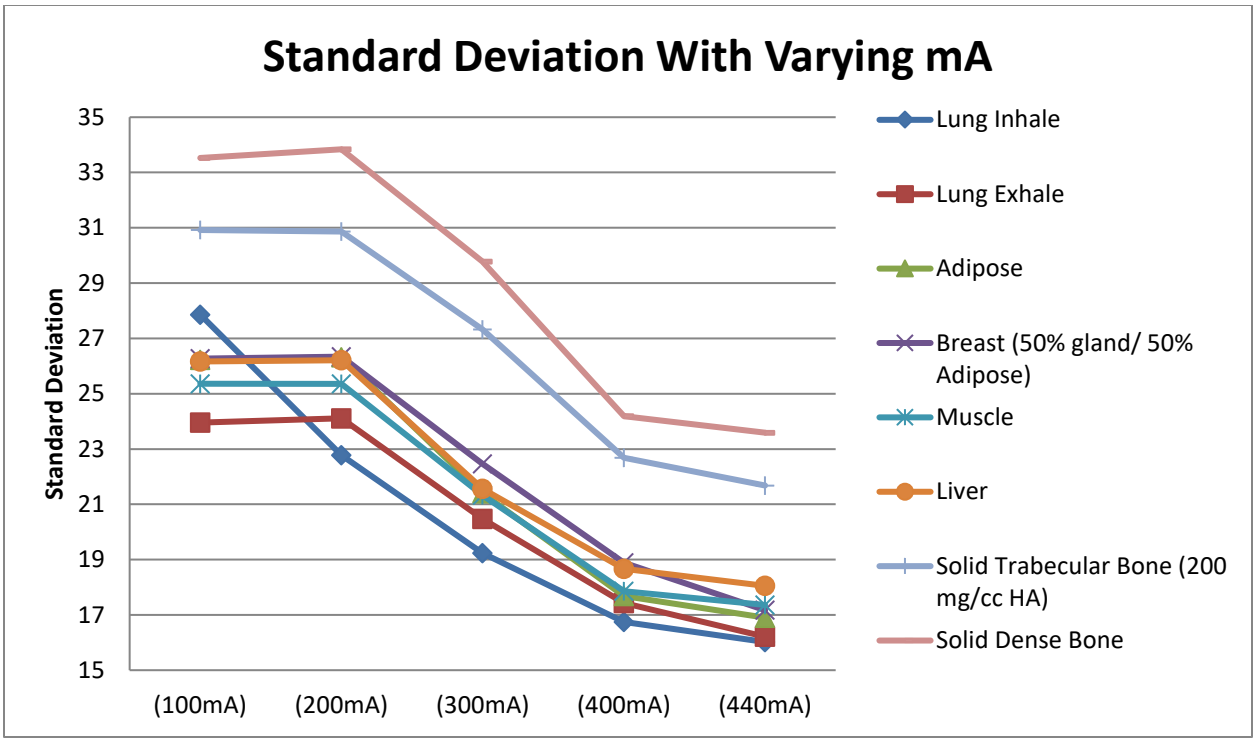

Figure 11: Changes in mA and the corresponding change in Standard Deviation.

Discussions

CT images are susceptible to a partial volume effect stemming from variations in patient's cross-section perpendicular to the scan direction. This has a direct effect causing systematic errors in voxels and huge variations in density. Each detected signal for a specific line between the x-ray source and the detector consist of three components; the primary beam attenuated by the patient, the Compton scattered radiation and the Coherent scattered radiation [6]. These parameters are all normalized to the detector signal in the absence of a patient. The accuracy of CT-ED_r calibration is a key component for dose calculation in inhomogeneous media. The tolerance levels of ED_r ensure the suitability of CT-ED calibration table of planning CT and CBCT. The relationship between the dose error ΔD and the error in ΔED_r is given by:

$$\Delta ED_r = \frac{\Delta D/D}{t_i} \frac{TMR}{\left(\frac{dTMR}{d(d_{eff})}\right)} \qquad (4)$$

Where:

ΔD/D - is the relative dose error to local dose

TMR/dTMR/ $d_{(deff)}$ - is the gradient of TMR relative to the local TMR

ΔED_r- is error in relative effective dose

T_i- is thickness of tissue

It was discovered that there was a corresponding decrease in HU with increases in kVp due to the increase in photon energy. The HU value generated per pixel for a CT scan is a direct result of the linear attenuation

DOI: *https://doi.org/10.52793/JCTR.2021.1(1)-08*

of the photon beam as it traverses the patient and the resultant energy with which it interacts with the detectors. Increasing the tube voltage increases the penetrating power of the rays and therefore, they can traverse the tissue with less attenuation (absorption and scatter), resulting in more beamlets reaching the detector with higher energies. The net increase of photon-detector interaction decreases image noise (SD). This occurs due to the increased photon intensity per pixel resulting in an improved contrast to noise ratio.

It should be noted that noise reduces the contrast between tissues with similar densities because it limits low contrast resolution, and sometimes masks anatomy with similar density to surrounding tissue. Therefore, this improvement will make tissue differentiation even easier leading to more accurate delineation of contours and resultant dose calculations. It should be highlighted that increasing the kVp also increases the probability of the Compton Effect and the generation of Bremsstrahlung interactions. A high energy photon may possess enough energy to surpass orbital electrons and be influenced by the nucleus of an atom. Here it slows down (lose energy in the form of a photon) and change direction. This particle and the resultant scattered photon can move on to interact with orbital electrons of the same atom or some other atom. If the scattered photon possesses enough energy it may also interact with the nucleus of another atom generating more photons. This causes a net increase in the number of photons reaching the detector, which is a secondary contributor to image density.

The change in mA showed negligible changes in HU because the energy of the photons generated was not increased; therefore, they were all subjected to similar linear attenuation resulting in similar HU values. The resultant decrease in SD with increases in mA can be attributed to increases in image density. Increases in mA cause the filament temperature to increase, thus increasing the rate of thermionic emission. With more electrons being released from the cathode within a given time frame, the frequency of collision between the electrons and anode increase; thus, more x-ray photons are released. As the number of photons increase, a specific volume of tissue is exposed to more beamlets within that time frame. Also, more photons are available to interact with the detector creating more density which manifests as a decrease in the SD. It is thus evident that increases in mA increase patient dose and the absence of digital image correction factors would result in an overexposure.

Compared to muscle/organ tissues, adipose/marrow tissues have a high concentration of fat. Connective tissue have a high concentration of collagen, teeth have a high concentration of minerals and bones are somewhere between these two extremes. The concentration of these individual tissues varies, giving rise to different densities accounting for tissue differentiation on scanned images. The location of these densities next to each other creates interfaces that influence the level of attenuation of kilo voltage photons or the beam fluency of megavoltage treatment particles [7]. Hughes in their study argued that CT-ED calibration curve is dependent on the matrix size used in the reconstruction. It was observed that when the matrix size increased there was corresponding reduction in HU. This study also proved that the reconstruction smoothing kernel affects the CT-ED calibration, as binning, averaging and diffusion filtering on raw data projections influences HU and the equivalent signal to noise ratio. This variation implies that a dose calculation error could result should a different smoothing kernel or reconstruction matrix size be utilized for a scan that was used for CT-ED calibration.

DOI: *https://doi.org/10.52793/JCTR.2021.1(1)-08*

Conclusion

From this study, "dose variation was found to be well within 2% of the expected dose". Therefore, it can be concluded that the clinical practice of employing 120 kVp for CT image acquisition is viable for radiation therapy dedicated simulations. The balance between the image quality and the dose delivered to the patient is an extremely important factor during image acquisition. The selected scan parameters have a direct impact on the image quality. The agreement in the selection of scan parameters influences deviations from the TPS HU-ED_r calibration curve that may lead to uncertainties in the calculation of output dose in the radiotherapy plan. These errors are manifested as poor precision and accuracy (overdose or under dose) in the delivered dose, leading to suboptimal tumor response or additional complications. Therefore, any attempts to link HU changes to TPS dose changes must consider the algorithm used for calculation and the anatomical region of interest. The articles reviewed suggest that the following HU tolerances could be set to achieve a 1% dose change limit: ±20 HU for soft tissue and ±50 HU for lung and bone. Some publications propose that it may be possible to allow a higher change than this for bone and still remain within 1% for dose change, which is caused by calibration errors of CT-ED10 [8]. Therefore, it is clear that accurate TPS calibration is critical for accurate dose determination and best tumor control outcomes [9-12].

Acknowledgement

The authors wish to acknowledge the management and staff of the National Cancer Treatment Centre of the Ministry of Health and Wellness where scanning and image analysis were done, for their cooperation and contribution to this study. Gratitude is also conveyed to Mr. Corey Drakes for his valuable contribution and discussion. Acknowledgement is due to the International Atomic Energy Agency (IAEA) for the support provided through the National and Regional Technical Cooperation programs.

References

1. Jones KC, Redler G, Templeton A, Bernard D, Turian JV. (2018) Characterization of Compton- Scatter imaging with an analytical simulation method. PHYS MED BIOL. 63(2):025016.
2. Khan FM, Gibbons JP. (2014) Khan's the physics of radiation therapy. Lippincott Williams & Wilkins.
3. Huizenga H, Storchi PRM. (1985) The use of computed tomography numbers in dose calculations for radiation therapy. Acta Oncol (Madr). 24(6):509-19.
4. Kanematsu N. 2015. Relationship between mass density, electron density, and elemental composition of body tissues for Monte Carlo simulation in radiation treatment planning. arXiv preprint. arXiv:1508.00226.
5. Koniarova I. (2019) Inter-comparison of phantoms for CT numbers to relative electron density (RED)/physical density calibration and influence to dose calculation in TPS. J Phys Conf Ser. 1248(1).
6. Nakao M, Ozawa S, Yamada K, Yogo K, Hosono F, et al. (2018) Tolerance levels of CT number to electron density table for photon beam in radiotherapy treatment planning system. J Appl Clin Med Phys. 19(1):271-75.
7. Hughes J, Holloway LC, Quinn A, Fielding A. (2012) An investigation into factors affecting electron density calibration for a megavoltage cone-beam CT system. J Appl Clin Med Phys. 13(5):93-107.
8. Fang R, Mazur T, Mutic S, Khan R. (2018) The impact of mass density variations on an electron Monte Carlo algorithm for radiotherapy dose calculations. Phys Imaging Radiat Oncol. 8:1-7.
9. Hunemohr N, Paganetti H, Greilich S, Jakel O, Seco J. (2014) Tissue decomposition from dual energy CT data

for MC based dose calculation in particle therapy. Med Phys. 41(6):1-14.

10. Thomas SJ. (1999) Relative electron density calibration of CT scanners for radiotherapy treatment planning. Br J Radiol. 72(86.):781-6.
11. Siegel MJ, Schmidt B, Bradley D, Suess C, Hildebolt C. (2004) Radiation dose and image quality in pediatric CT: Effect of technical factors and phantom size and shape. Radiol. 233(2):515-22.
12. Brisse HJ, Aubert B. (2009) CT exposure from pediatric MDCT: results from the 2007-2008 SFIPP/ISRN survey. J Radiol. 90(2):207-215.